



Contents lists available at ScienceDirect

Arabian Journal of Chemistry

journal homepage: www.sciencedirect.com



Original article

Selection and evaluation of biomarkers of *Gynostemma pentaphyllum* (Thunb.) Makino representing its tonifying weakness and strengthening muscle effect based on PXR/IL-6/SERCA1a regulation

Houran Cao^{b,1}, Dongmei Li^{a,c,1}, Guangying Wu^{a,c}, Peihong Chen^d, Guanlin Xiao^{a,c}, Xiaoli Bi^{a,c,*}, Zhao Chen^{a,c,*}^aThe Fifth College of Clinic Medicine, Guangzhou University of Chinese Medicine, 60 Hengfu rd, Guangzhou 510095, China^bThe Second College of Clinic Medicine, Guangzhou University of Chinese Medicine (Guangdong Provincial Hospital of Chinese Medicine), 111 Dade rd, Guangzhou 510120, China^cGuangdong Provincial Key Laboratory of Research and Development in Traditional Chinese Medicine, 60 Hengfu rd, Guangzhou 510095, China^dYantian District People's Hospital of Shenzhen City, 2010 Wutong rd., Shenzhen, 518081, China

ARTICLE INFO

Article history:

Received 14 March 2023

Accepted 20 September 2023

Available online 28 September 2023

Keywords:

Gynostemma pentaphyllum (Thunb.) Makino

PXR/IL-6/SERCA1a

Metabolomics

Tonifying weakness and strengthening muscle effect

ABSTRACT

TCM internal medication is usually beneficial after muscle injury or pulling, among which *Gynostemma pentaphyllum* (Thunb.) Makino (Gyp) has shown good activity; however, an explanation and evaluation of its therapeutic effect is needed. The problem lies in the fact that the main regulatory pathway for Gyp is unclear, lacking scientific and systematic mechanisms and standards. It was reported in our previous paper that components in Gyp regulate the expression of the PXR/IL-6/SERCA1a signaling pathway to achieve such therapy, but there remains a lack of an accurate method and standard for evaluation. In this study, based on our previous discovery, a relatively comprehensive and accurate investigation was carried out to establish the metabolomic profile of Gyp's therapeutic effect. Metabolomics studies showed that a total of 49 different metabolites were found, of which 24 were related to PXR-IL-6-SERCA1a, and they were mainly involved in skeletal muscle cell repair, material and energy metabolism, and inflammatory response, which not only provides accurate standards for PXR/IL-6/SERCA1a regulation but also explains its tonifying weakness and strengthening muscle effect in TCM theory in a scientific and quantitative way.

© 2023 The Author(s). Published by Elsevier B.V. on behalf of King Saud University. This is an open access article under the CC BY-NC-ND license (<http://creativecommons.org/licenses/by-nc-nd/4.0/>).

1. Introduction

Gynostemma pentaphyllum (Thunb.) Makino (Gyp) is an herbal TCM with Lingnan characteristics that is used by locals for muscle injury, weakness, cough and hyperlipidemia (Alhasani et al., 2020; Weng, et al., 2021; Shen, et al., 2019). In TCM theory, Gyp is defined as “cold” and “bitter”, with effects such as strengthening Qi, moistening the lung and lowering lipids. To be specific, “cold” and “bitter” means lowering the inflammation and blood viscosity levels in

body, alleviating oxidative stress and pain, along with promoting circulation; such effects improve amino acid, protein and energy generation and transportation, which is corresponding with invigorating qi. Our previous studies indicated that this herb shows good activities for lowering blood lipids and muscle injury (Chen et al., 2022a, 2022b, 2021). However, the articles mentioned above mainly focused on active components in Gyp, and targets with direct regulatory effects on skeletal muscle were not accordingly evaluated (Yang et al., 2013). Furthermore, the comprehensive signaling mechanism and changes in metabolites in the course of skeletal muscle recovery still need investigation. In general, the biological basis of Gyp's activity is the key to strengthening Qi, moistening lung and lowering lipid effects described in classic TCM works, giving more scientific and medical meaning to Gyp (Chen et al., 2022a, 2022b; Liu et al., 2022b).

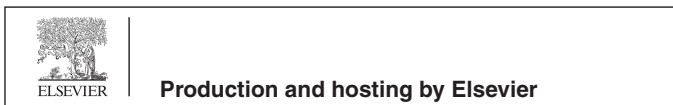
Regeneration of muscle is regulated by certain pathway(s) that control energy (ATP) and protein (by affecting amino acid levels), along with the concentration, transportation and emission of inflammatory factors (Panci and Chazaud, 2021; Sikorska et al.,

* Corresponding authors at: 60 Hengfu rd, Guangzhou, 510095, China.

E-mail addresses: bixiaoli1234@hotmail.com (X. Bi), cz04101103@hotmail.com (Z. Chen).

¹ Equal contributor.

Peer review under responsibility of King Saud University.



2021; Jiang et al., 2020). The mechanism for the abovementioned change is components in the herb extract (Gyp, for instance) taken by the body first affiliated with several core receptors, such as PXR and NF- κ B, followed by a series of changes caused by the regulation of those receptors (Zhang, et al., 2020; Hassani-Nezhad-Gashti, et al., 2018; Wu, et al., 2018). In particular, as the literature indicates, PXR plays a more important role in the skeletal muscle recovery process than other core receptors because PXR has a stronger regulatory effect on energy, lipid metabolism and the concentration of inflammatory factors (Hakkola, et al., 2016; Bitman, et al., 2011). Variation in interleukins (ILs) is usually observed when injury occurs, among which IL-6 is reported to have an important role in skeletal muscle, and its concentration significantly changes when injury occurs in the latter, making it a suitable indicator for evaluation of the injury degree and recovery. Additionally, regulation of PXR influences the generation, concentration and transportation of IL-6 by reducing its synthesis and promoting its excretion at the same time. The inflammatory effect in the injured part will be alleviated by changes in PXR expression (Kaur, et al., 2020; Camejo et al., 2020; Pant, et al., 2016).

SERCA is widely distributed in skeletal, cardiovascular, and visceral smooth muscles and regulates calcium concentrations in and outside the sarcoplasmic reticulum. Among several subtypes (SERCA1-3), SERCA1a is mainly distributed in adult skeletal muscle. Studies have shown that high expression of this target can stimulate Ca²⁺ influx and ATP metabolism, increase skeletal muscle energy consumption and accelerate muscle tissue growth (Oliva et al., 2021; Tanihata, et al., 2018; Nelson, et al., 2016). Therefore, the changes in SERCA1a under the influence of drugs are of great scientific significance for the study of the mechanism by which Gyp promotes muscle injury repair. The relationship between PXR and SERCA1a has been reported by several groups, confirming the mechanism of these targets in skeletal muscle recovery (Zhou, et al., 2021; Won et al., 2019). Therefore, the PXR-SERCA1a pathway can be used to explain the biological basis of Gyp's TCM-based effect along with the PXR/IL-6 mechanism.

Studies have shown that some endogenous substances, such as bile acids LCA and CDCA, CDA, and CA, can be combined with PXR and show some regulatory effects, inducing activity changes, adjusting interleukin, tumor necrosis factor, ceramide, and prostaglandin levels, as well as a series of messengers or ligands in the body. These compounds associate with IL-6 metabolic regulatory enzymes and play a role in changing its concentration, transport and distribution in vivo (Biagioli and Fiorucci, 2021; Ticho et al., 2019; Zhang, et al., 2018). Similarly, changes in the expression of the latter can lead to changes in the synthesis, transport, and metabolism of a series of transmitters (e.g., apolipoprotein SLN) and ultimately affect the activity of regulatory proteins such as SERCA1a that are widely distributed in muscle tissue (Liu et al., 2020; Chen et al., 2020; Kumar and Muthu, 2015). Therefore, the use of metabolomics methods and techniques to screen and measure endogenous components of the regulatory activity of various relevant targets under Gyp intervention is helpful to clarify the signal transduction mechanism of drug action and to establish the precise and quantifiable biological relationship between the macro dialectic of TCM and the micro response/reaction of molecular biology (Liu et al., 2021a; Ilaiwy, et al., 2019).

Generally, active compounds in the herb such as Gyp was first affiliated with PXR. As a nuclear receptor with obvious energy and lipid regulation activities, PXR is widely distributed in kidney, spleen, liver and other organs, and its expression changes can also accurately characterize the function and operation of these organs. According to TCM theory, kidney and spleen is the "regulator" of bone and muscle conditions, and Gyp can be categorized to lung, spleen and kidney channels. The selection of PXR can better explain the molecular biological basis of the therapeutic efficacy

of Gyp, and clarify the molecular mechanism of the holistic and related treatment of TCM (Cao, et al., 2022; Ihunnah, et al., 2011). As an important factor regulating inflammation in the body, IL-6 is significantly affected by changes in PXR activity (Bautista-Olivier, et al., 2022; Yue, et al., 2021). In addition to affecting the regeneration of skeletal muscle cells by regulating the level of inflammation at the injured site, IL-6 can also play a direct and indirect regulatory role on SERCA1a and other related receptors and physiological factors. SERCA1a is widely distributed in adult skeletal muscle and is an important regulatory site for skeletal muscle movement, repair and metabolism. Studies have shown that this target may be regulated by upstream genes such as PXR. By studying the process of PXR regulating SERCA1a activity through IL-6 under the intervention of Gyp (Panci and Chazaud, 2021; Qaisar, et al., 2019), we can better understand the mechanism of gynostaphyllus promoting skeletal muscle cell regeneration, establish the correlation between PXR/IL-6/SERCA1a expression and muscle strain repair, and finally clarify the pharmacodynamic mechanism to provide scientific and accurate explanation for the efficacy of traditional Chinese medicine.

At the same time, Gyp can tonify deficiencies in the spleen and kidney and promote repair of muscle strain, which involves energy and a variety of nutrients and raw materials required for cell differentiation and regeneration. The changes in these endogenous substances and their tissue distribution can provide a scientific basis for the study of the metabolic mechanism of the body under drug intervention and quantitative standards for the evaluation of disease course. Therefore, in addition to messenger and transmitter components, metabolomics studies can also screen out "raw materials" related to the abovementioned benefits and repair. By comparing the differences in the abovementioned components in different animal experimental groups (control, model and administration), we can further clarify not only the mechanism by which Gyp regulates the expression of PXR/IL-6/SERCA1a and promotes the repair of muscle strain but also its relationship with tonifying and strengthening muscle.

In summary, this manuscript reports our investigation of the biological and scientific link between Gyp's skeletal muscle recovery effect, which is based on the TCM theory that described the former as tonifying weakness and strengthening muscle activities, and our previous study of components with PXR/IL-6 regulatory effects. Changes in the target expression of the PXR/IL-6/SERCA1a pathway accompanied by the discovery of related metabolites and their variation in the course of Gyp therapy provided solid ground for explanation of its mechanism, which provides insight into understanding the inherent law of TCM.

2. Instruments, materials, and methods

2.1. Instruments

Metabolite identification and acquisition of the metabolomic profile were carried out by AB SCIEX Triple TOF 5600 + UHPLC-TOF-MS (AB SCIEX, Framingham, MA, USA). Subsequent determination of the abovementioned components in vivo was performed in a Thermo-TSQ quantum mass spectrometer (Thermo-Fisher, San Jose, USA) fitted with a Phenomenex C18 column (2.1 × 50 mm, 5 μ m, Torrance, CA, USA). For biochemical investigation, PCR analysis for PXR expression in different experimental groups was performed using an IQTM5 fluorescence quantitative PCR instrument (Bio-Rad, Hercules, CA, USA). ELISA determination of IL-6 expression was performed in a Varioskan Flash Fluorescence microplate reader with the help of the SimpleStepTM tool kit purchased from Abcam (Waltham, MA, USA). SERCA 1a expression was detected by western blot with a Varioskan Flash Fluorescence microplate

reader. For details of the primers, antibodies and other materials and reagents, see the corresponding sections describing those experiments. Sample pretreatment used the following instrument: MD 200 sample concentrator (Aosheng Instruments, Hangzhou, China), Thermo Legend Micro 17R low temperature high speed centrifuge, and a Thermo 88,880,018 Vortex (Thermo-Fisher, San Jose, USA). The deionized water was prepared by using a Milli-Q system (Millipore, MA, USA), and all weighing was done using an XS205DU scale (METTLER TOLEDO, Zurich, Switzerland).

2.2. Materials and reagents

RIPA protein lysis solution (Solebo Technology Co., LTD, Beijing, China), Multi Imaging System (Tanon, Shanghai, China), predyed Rainbow protein Ma (Thermo-Fisher, San Jose, USA), Bicinchoninic Acid protein Kit (Thermo-Fisher, San Jose, USA), mouse monoclonal β -actin antibody (Dingguochangsheng Biotechnology Co., LTD, Beijing, China), Goat Anti-mouse antibody (Proteintech, Hamburg, USA), PXR antibody (Proteintech, Hamburg, USA), SERCA antibody (abcam, Cambridge, Britain), TRIZOL RNA lysate (Ding Guochangsheng Biotechnology Co. LTD, Beijing, China); PerfectStart Green qPCR SuperMix (TransGen Biotech Co., LTD, Beijing, China), Evo M-MLV RT Premix for qPCR (Ecorui Bioengineering Co., LTD, Hunan, China). The reagents used in the biochemical experiment and mass analysis, including acetonitrile, formic acid, methanol, ethanol, and DMSO, all of HPLC grade, were purchased from Merck (Darmstadt, Germany). Celecoxib capsules (200 mg/capsule) were purchased from Pfizer (New York, United States); Gynostemma pentaphyllum decoction pieces were purchased from Zhixin Pharmaceutical Co. Ltd. (Guangzhou, China).

2.3. Animal experiments

Thirty-six healthy male SD rats weighing 300 ± 20 g, SPF grade (Certificate: SCXK (Xiang) 2019-0014, purchased from Changsha Tianqin Biotechnology Company), were used for pharmacological experiments. The rats were fed under laboratory conditions (room temperature $22 \sim 225$ °C, relative humidity $55 \sim 70\%$), and all experiments and animal welfare were supervised by the ethical committee of the Fifth Clinical College of Guangzhou University of Chinese Medicine. Preparation of blunt injury of rat skeletal muscle followed the procedure below: The modeling was performed in a blunt contusion model impact device. Twenty-four hours before modeling, the hair of both lower limbs of the rats was shaved with an electric shaving knife, and the rats were anesthetized with ether. Then, the rats were fixed on the rat plate in a prone position, with knee extension and ankle flexion of the right lower limb at approximately 90° to fully expose the gastrocnemius muscle, and the hind limbs were padded with gauze pads to avoid fracture during modeling. The head of the blow device was pressed close to the middle abdominal segment of the gastrocnemius muscle, and finally, the muscle abdomen was hit once with the free fall motion of heavy objects, resulting in closed blunt contusion of the gastrocnemius muscle in rats. The criteria for successful modeling were as follows: ① There was no open damage of the skin at the strike site of the right hind limb, subcutaneous bleeding and ecchymosis, induration mass at the strike site, or notable swelling compared with the left hind limb. ② After modeling, the rats could walk, but their gait was slightly lame, and the right hind limb was weak in grasping the bar when climbing the bar. The model animals were divided into the following groups (6 for each): ① sham group, no further treatment was performed in the rats; ② positive control group, the animals were given 72 mg/kg celecoxib; ③ Gyp low dose, the rats were given the Gyp extract (Gynostemma pentaphyllum extracted by ethanol using heat reflex, made into dried extract) equivalent to 437.5 mg/kg of the crude drug; ④

Gyp medium dose, the rats were given the Gyp extract equivalent to 875 mg/kg of the crude drug; ⑤ Gyp high dose, the rats were given the Gyp extract equivalent to 1750 mg/kg of the crude drug; and another 10 normal rats were selected as the blank group. The rats in each administration group were given the corresponding drugs by intragastric administration at a weight of 10 mL per animal, while the blank and model control groups were given the same volume of purified water. The drug was administered by gavage once a day for 30 days. During the administration, all rats took food and water normally. One hour after the last administration, the animals in each group were humanely killed after anesthesia, and whole blood was collected for serum separation and frozen at -80 °C for future use. The skeletal muscle, liver, kidney, and spleen of the injured side of the thigh were taken. Part of the tissues were used for pathological examination, and the remaining tissues were frozen at -80 °C for future use.

2.4. Detection and analysis of PXR/IL-6/SERCA1a expression

For PXR and SERCA1a expression, RT-PCR methods were developed and optimized. The procedures were similar overall with differences in primers: 50 mg of homogenate tissue (spleen, kidney, liver and skeletal muscle) was taken from rats of different groups into a grinding tube, and then 0.5 mL of TRIZOL reagent was added for grinding. Centrifugation was performed at 12,000 RPM at 4 °C for 10 min. The resulting supernatant was transferred to a 1.5 mL centrifuge tube, followed by the addition of 100 μ L of chloroform, and then the mixture was shaken vigorously for 2 min. Then, it was centrifuged at 12,000 RPM at 4 °C for 10 min. The resulting supernatant was transferred to a new 1.5 mL centrifuge tube, and isopropyl alcohol was added in equal volume. The mixture was placed in the refrigerator at -40 °C overnight and subsequently centrifuged at 12,000 RPM at 4 °C for 10 min. The supernatant was discarded, and the precipitate was kept and washed twice with 0.5 mL of 75% ethanol and then dried for 20 min at room temperature. The obtained matrix was added to 50 μ L of ddH₂O, and 5 μ L of the solution was mixed with 195 μ L of sterilized water. The mixture was measured for the OD260/OD280 ratio by a nucleic acid protein analyzer. The concentration and purity of RNA were calculated according to the analysis results. For gene expression, first strand cDNA was synthesized by reverse transcription. Using cDNA as a template, specific primers were designed according to the gene sequence, and the expression of each gene was detected by PCR.

Determination of IL-6 concentration was carried out by the method used in our previous experiment: samples obtained in the "Animal experiment" section were extracted for total RNA by TRIZOL reagent, and reverse transcription was performed by a SuperScript™ VILO™ cDNA Synthesis Kit, followed by qPCR (detecting PXR expression) using TaqMan gene expression assays (Applied Biosystems, Carlsbad, CA, USA) guided by the instructions. For IL-6 determination, ELISA was carried out according to the manufacturer's instructions.

The obtained data of the abovementioned experiments were statistically compared between groups (blank vs. model, model vs. prescription groups), and the results will help understand the activity mechanism of GYP, as well as the metabolites responsible for it.

2.5. Identification and analysis of related metabolites

Biological samples such as serum, skeletal muscle, liver, kidney and spleen were taken from the "animal experiment" part and transferred to a 1.5 mL EP tube according to 100 μ L of serum or homogenate tissue sample, and 400 μ L precooled methanol was added. The acetonitrile mixture (1:1) was vortexed for 30 s, placed

in a -20°C refrigerator for 1 h, and centrifuged at 12,000 RPM for 15 min at 4°C , and 400 μL supernatant was taken and placed into a 1.5 mL EP tube. The extracted supernatant was dried by nitrogen, 100 μL of precooled acetonitrile:water mixture (1:1) was added to the residue, and the mixture was vortexed for 30 s. Finally, the sample solution was centrifuged (4°C , 12,000 RPM) for 15 min, and 80 μL of the supernatant was taken for UPLC-TOF-MS analysis. The UPLC-TOF-MS analysis used the following chromatographic conditions: a Waters HSS T3 column (100×3.0 mm, $1.8 \mu\text{m}$) was used with a mobile phase consisting of 0.05% formic acid (A) and acetonitrile (B). The gradient elution procedure was 0 ~ 1.0 min, 3% B; 1.0 ~ 10 min, 3 ~ 30% B; 10 ~ 20 min, 30 ~ 99% B; 20 ~ 26 min, 99% B; and 26 to 26.1 min, 99 ~ 3% B. The column temperature was 40°C , and the flow rate was 0.4 mL/min. The following mass conditions were used: positive and negative ions were simultaneously scanned, and the mass charge ratio was in the range of 50–1000 Da. The spray voltage was 5000 V, and the vaporization temperature was 550°C . The collision was 35 eV, the dissociation voltage was 60 V, the atomized gas (Gas1) was 379.23 kPa, the auxiliary gas (Gas2) was 379.23 kPa, and the curtain gas (CUR) was 341.33 kPa. The remaining settings were instrument presets. After analysis, the acquired atlas and data were imported into AB Sciex Analyst Software 1.6 for analysis, and its standard procedure was used to identify the peaks to provide metabolites information (ion pair and retention time).

2.6. Explaining Gyp's therapeutic effect based on metabolomics

The obtained results mentioned in the "Identification and analysis of related metabolites" section were first sorted and transformed into a format suitable for the SIMCA software package (version 14.1, Umetrics, Sweden). The following statistical analysis was performed: the first matrices step Pareto scaling (par transformation); then, multivariable statistics, such as principal component analysis (PCA), partial least-squares discrimination analysis (PLS-DA), and orthogonal projections of latent structures discriminant analysis (OPLS-DA), by which the relationship among experimental groups, as well as differences in the forms of the type and content of the metabolites, was determined.

The permutation test was used to validate and evaluate the established OPLS-DA model, and the significance of each variable was evaluated using Student's *t* test, followed by categorizing of the processed values using criteria described below: metabolites with variable importance in projection (VIP) values > 1.0 in the

OPLS-DA model and $p < 0.05$ in the *t* test were selected as candidate biomarkers, while those without these values were excluded. Furthermore, $|P(\text{corr})| \geq 0.5$ in the S-plot was set as the standard for the variables, and the values fulfilled were regarded as those most correlated with OPLS-DA discriminant scores. By this step, the possibility of selecting a false biomarker candidate was significantly reduced.

Peaks detected in UPLC-TOF-MS analysis were processed using MS-Dial (version 3.7) to identify metabolites in the peaks of the TIC chromatogram, and the given prediction was analyzed in combination with related literature. Raw data acquired from MS were converted using an ABF converter (<https://www.reifycs.com/AbfConverter/>) before being imported into MS-Dial. Data analysis parameters were as follows: RT, 0–30 min; mass range, 50–1000 Da; MS1 tolerance, 0.01 Da; and MS2 tolerance, 0.05 Da. The parameters for peak detection were as follows: smoothing method, linear weighted moving average with smoothing level of two scans; minimum peak width, five scans; minimum peak height, 1000 amplitude; mass slice width, 0.1 Da; and exclusion mass list, none. The parameters for metabolite identification were RT tolerance, 2 min; MS1 accurate mass tolerance, 0.01 Da; MS2 accurate mass tolerance, 0.05 Da; and identification score cut off, 80%. Using the databases Human Metabolome Database (HMDB) (<https://www.hmdb.ca>), Metlin (<https://metlin.scripps.edu/>), LIPID MAPS (<https://www.lipidmaps.org/>) and Massbank (<https://massbank.eu/MassBank/>), the MS and MS-MS spectra were accurately compared to identify metabolites in the process of MS Dial analysis. Metabonomics information was obtained through Metaboanalyst 5.0 (<https://www.metaboanalyst.ca/faces/home.xhtml>) to determine the potential mechanism and dynamics. The threshold of pathway impact (calculated from topology analysis) was set as 0.1, and values above that were selected as potential signaling pathways.

Metabolites with an obvious relationship with the PXR/IL-6/SERCA1a pathway were selected as indices for accurate content determination using a Thermo-Fisher TSQ Quantum UHPLC-MS-MS instrument (Thermo Fisher, San Jose, United States). The chromatographic conditions were: solid phase using a Phenomenex C18 column (2.1×50 mm, $5 \mu\text{m}$, Torrance, CA, USA); mobile phase containing 0.1% formic acid (A) and acetonitrile (B), the elution used gradient mode, program set as follows: 0–1 min, 5%–5%B; 1–1.5 min, 5%–90%B; 1.5–2.5 min, 90%–90%B; 2.5–3 min, 90%–5%B. The mass detection was operated under ESI mode, collecting both negative and positive ions. The spray voltage was 3500 V,

Table 1
Optimum conditions of Mass conditions for metabolites.

Compound	Parent (m/z)	Fragment	Retention time (min)
DI-Glutamic acid	146.0454	102.0547, 128.0342	0.8570
N-ACETYLNEURAMINATE	308.0984	307.0984	0.9740
Cytidine	244.0920	196.8839, 152.8945, 130.8770	1.1750
Nicotinamide	123.0548	96.0449, 78.0345, 106.0280	1.2170
Hypoxanthine	137.0451	87.0076, 75.0088, 59.0164	1.2340
Xanthine	153.0402	152.0402	1.3110
L-Methionine	150.0581		1.6510
Uridine	245.077	110.0235, 82.0285, 200.0558	1.8130
Tyrosine	182.08093	163.0397, 136.0766, 119.0501	2.0090
L-Phenylalanine	166.0858	147.0442, 96.9589, 136.9311	4.8910
GUANIDINOACETATE	118.0648	117.6480	5.3230
L-Tryptophan	205.0965	116.0493, 74.0234, 142.0651	5.3290
Riboflavin	377.1456	376.1456	5.7320
Creatine	132.0759	90.0546	7.170
Taurocholate	516.3002	80.2000, 106.9000, 124.1000	7.9340
Glycocholic acid	466.3177	446.2900, 402.2300, 382.2730	8.3930
1-Oleoyl- <i>sn</i> -glycero-3-phosphocholine	546.34691	190.2172	11.6950
Arachidonic acid	303.2321	302.2321	15.7840
9- <i>cis</i> -Retinal	285.2426	285.2426	15.8380
Palmitic acid	255.2331	171.1025, 255.4360, 237.4040	17.0990

the vaporization temperature was 350 °C, the capillary temperature was 300 °C, the sheath gas pressure was 30 psi, the auxiliary gas pressure was 10 psi, and the skimmer offset was 1 V. Parameters affecting the signal strength and specificity of each metabolite, including ion pair, tube length offset and collision energy, were optimized using TSQ matters software (Thermo-Fisher, San Jose, USA), and the optimum conditions for their detection are listed in Table 1, with a representative TIC chromatogram shown in Fig. 1. And validation was carried out to test the accuracy, reproducibility and stability of the analytical method, content and result see Tables S1–S7.

The peak area of each metabolite and standard obtained in the determination were calculated for their concentration in acquired biological samples (serum, skeletal muscle, kidney and intestine) of different groups. The differences between groups and their significance were determined by SPSS software according to the results of content determination, and the data revealed the regulatory mechanism of GYP on skeletal muscle recovery and the transportation of related metabolites.

2.7. Statistics and data processing

Calculation of the obtained data, including the results of pharmacodynamics, mRNA expression and metabolite contents, was performed using SPSS 20.0 (Chicago, IL, USA), and the results are presented as the mean \pm SD ($n \geq 3$). The statistical method used was one-way ANOVA followed by Dunnett's *t* test using SPSS. Groups of values with significant differences are marked as $p < 0.05$, while the opposite groups are marked as $p > 0.05$.

3. Results and discussion

3.1. Gyp's influence on skeletal muscle recovery

Judging from the evaluation criteria related to muscle strain and its degree of recovery, the animal model established in this study can successfully simulate the actual situation of muscle strain (Fig. S1). The pathological sections of the model group showed notable granulation tissue in sheets and edema, and partial muscle tissue was fractured, dissolved, and atrophied, indicating that the modeling was successful. After 30 days of administration, 83.33% of animals (5 for each group) in the middle- and high-dose groups of GYP met the relevant criteria for muscle recovery, which could be classified as rehabilitation. The proportion of recovered animals in the low-dose group was only 50% (3 animals); there was no significant difference between the medium- and high-dose groups and the positive drug group (5 animals recovered, accounting for 83.33%) ($p > 0.05$), but the latter was significantly better than the low-dose group ($p < 0.05$). At the same time, there were significant differences between the above experimental groups and the sham operation group (2 rats recovered, accounting for 33.33%), except for the low-dose GYP group, indicating that GYP could better promote the repair of muscle strain. The above results can also be confirmed by the pathological sections of each experimental group (Figs. 2–5). Fig. 3 shows that there was still obvious granulation and Henoch-purpura scar tissue, partial muscle cell rupture, and nuclear hyperplasia in the GYP low-dose group, which was not significantly different from that in the sham operation group; that is, it cannot be demonstrated that the damage can be repaired by administration at this dose. There was no abnormality in muscle

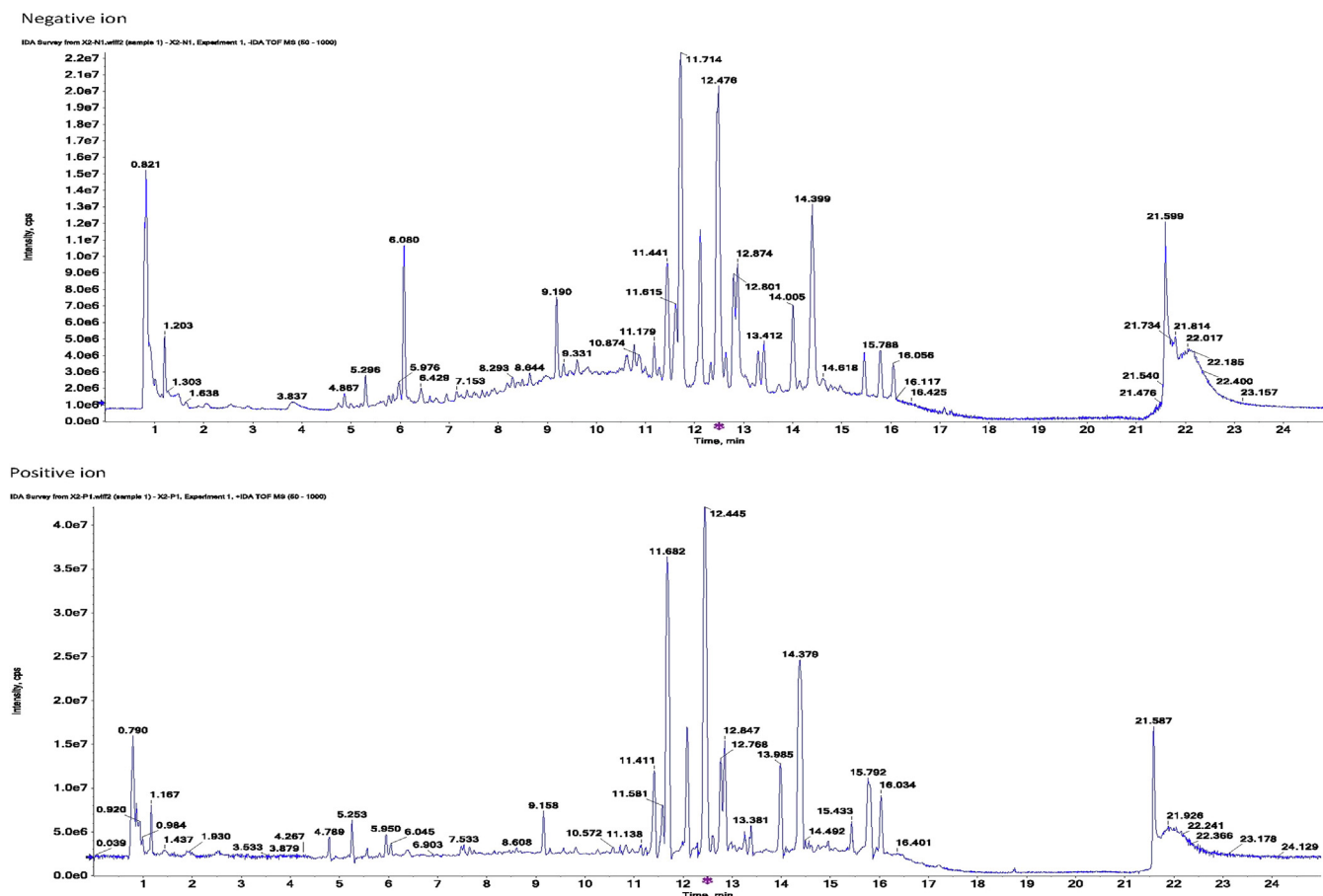


Fig. 1. Representative tic chromatogram for metabolomic samples (serum).

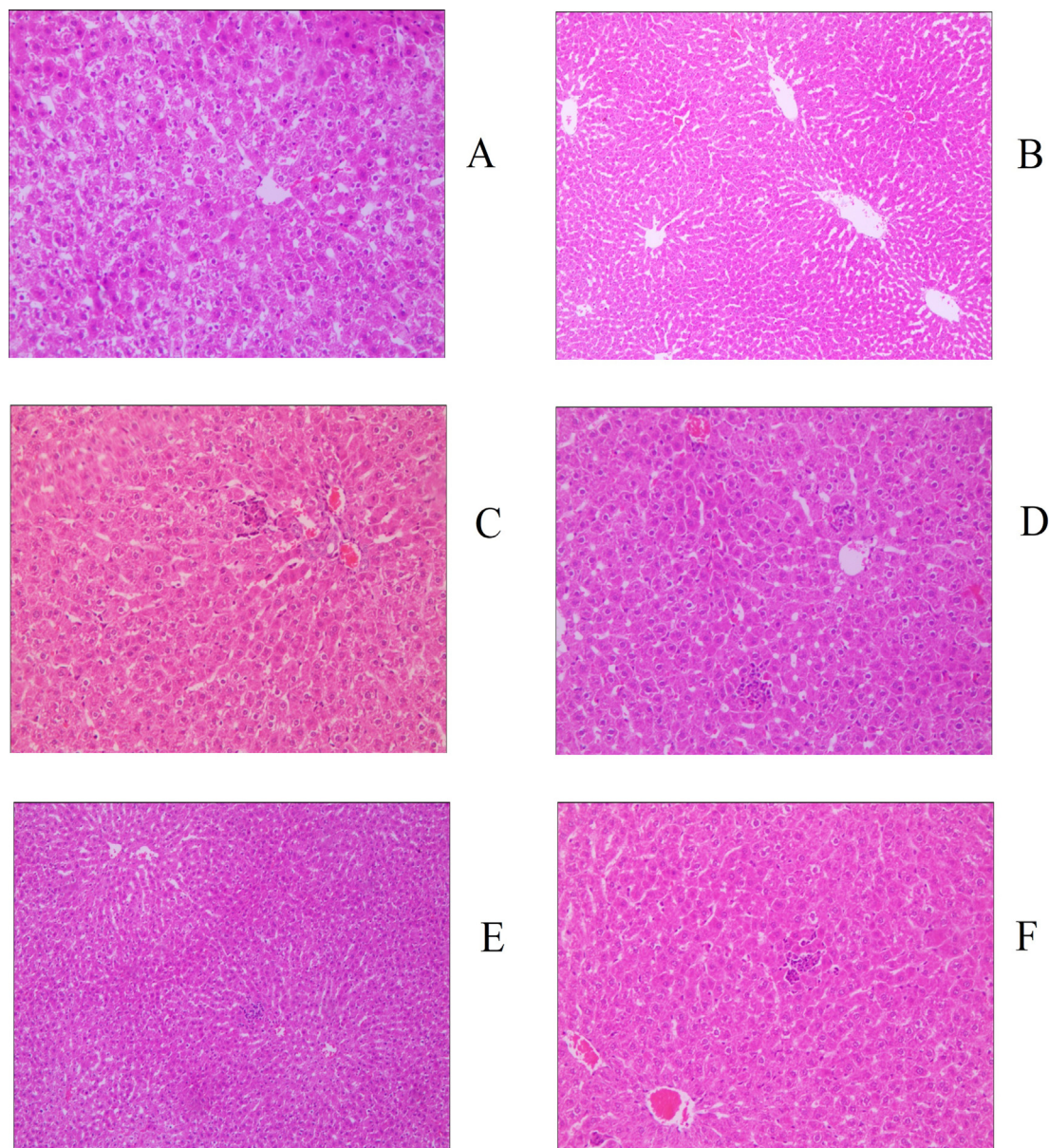


Fig. 2. Histology image of liver (200x), groups: a. blank, b. serum, c. positive control, d. gyp low dose, e. gyp medium dose, f. gyp high dose.

tissue or only a few atrophic cells in the medium- and high-dose groups of GYP and positive control, indicating that the repair of muscle strain was accelerated under the above dose/drug. In addition, the pathological sections of spleen, kidney, and other tissues also confirmed the discussion of the major muscles and bones of spleen and kidney in traditional Chinese Medicine to a certain extent (Fig. 4, Fig. 5). Figs. 4 and 5 show the presence of myofiber cells in both organ tissues of the abovementioned model/sham-operated groups, indicating fibrous tissue hyperplasia and impaired function in both organs. Although the above conditions were still observed in the medium- and high-dose GYP and positive control groups, the proliferation of fibrous tissue was significantly inhibited, indicating that organ function gradually returned to normal.

3.2. PXR/IL-6/SERCA1a assay results

For serum, the measurement results of PXR expression (Fig. 6) showed that the value in the sham operation group was significantly

lower than that in the blank group ($p < 0.05$), indicating that the expression of PXR decreased after modeling. The corresponding drug treatment can better inhibit the expression of PXR and promote the body to return to a normal state. Compared with the sham operation group, the results of the medium- and high-dose groups of GYP and the positive drug group were significantly different ($p < 0.05$), but compared with the blank group, there was no significant difference ($p > 0.05$). However, the above results were not observed in the low-dose GYP group, which had no significant difference from the sham operation group ($p > 0.05$) but did have a significant difference from the blank group ($p < 0.05$). From the observation of different matrices (blood/tissue samples), it can be seen that PXR expression in the sham group of the skeletal muscle was slightly lower than that in the blank group, while with no significant difference ($p > 0.05$). All medication groups (except GYP high) showed no obvious difference in the expression values but had a dose-dependent trend in the GYP groups. The changes in the liver in each experimental group were basically the same as those in the serum, but the kidney and spleen were irregular.

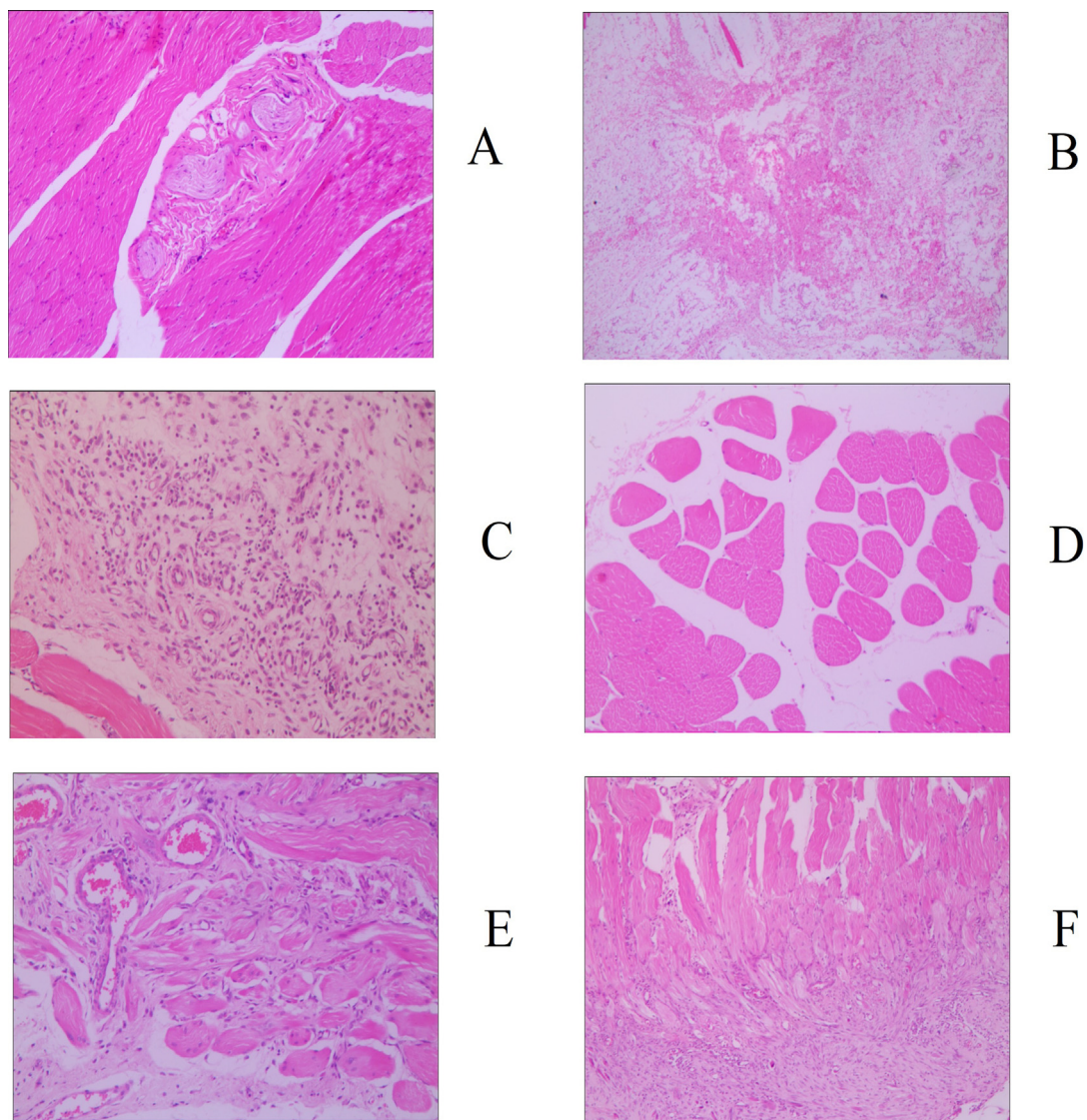


Fig. 3. Histology image of skeletal muscle (200x), groups: a. blank, b. serum, c. positive control, d. gyp low dose, e. gyp medium dose, f. gyp high dose.

Among the last two groups, the expression value of the medium-dose group of GYP was significantly lower than that of the low- and high-dose groups ($p < 0.05$), and there was no significant difference between the blank and sham operation groups ($p > 0.05$).

The results of the IL-6 assay were similar to those of PXR. The level of IL-6 in the organs (not in the serum, see Fig. 7) of the sham operation group was significantly increased, indicating that the high expression of PXR promoted the increase and enrichment of inflammatory factors. The medication can reduce the IL-6 level to different degrees. Fig. 7 shows that the measured values of the medium- and high-dose groups of GYP were significantly different from those of the sham operation group ($p < 0.05$). Although the relative expression value of GYP in the low-dose group in almost all matrices was lower than that in the sham operation group, it was not statistically significant compared with the latter ($p > 0.05$).

In terms of SERCA1a expression, the receptor had discernable tissue distribution specificity; except for skeletal muscle, the expression in other organs was irregular (Fig. 8), and there was no dose correlation among the GYP administration groups. The expression of SERCA1a in skeletal muscle was significantly damaged and regulated by drugs: the value of the sham operation group was significantly lower than that of the blank group

($P < 0.05$), while the GYP medium- and high-dose groups and the positive control could better restore the function of the receptor, and its expression value was significantly higher than that of the sham operation group ($P < 0.05$), which was similar to the level of the blank group. The expression of SERCA1a in the low-dose group was not significantly different from that in the sham-operated group ($P > 0.05$) and was still significantly higher than that in the blank group ($P < 0.05$).

3.3. Results of relevant metabolomic studies

Based on the abovementioned pharmacodynamic and molecular biological findings, it is concluded that GYP exerts its beneficial effects on muscle strain repair by modulating the PXR/IL-6/SERCA1a pathway. To better establish the biological basis of GYP for tonifying spleen and kidney deficiency according to this mechanism, we comprehensively analyzed the endogenous metabolites of animals in each experimental group, tried to determine the metabolites closely related to the expression changes of PXR/IL-6/SERCA1a key targets and established accurate determination methods for the contents of these metabolites in vivo (Fig. 1). The results were statistically analyzed to screen out the key meta-

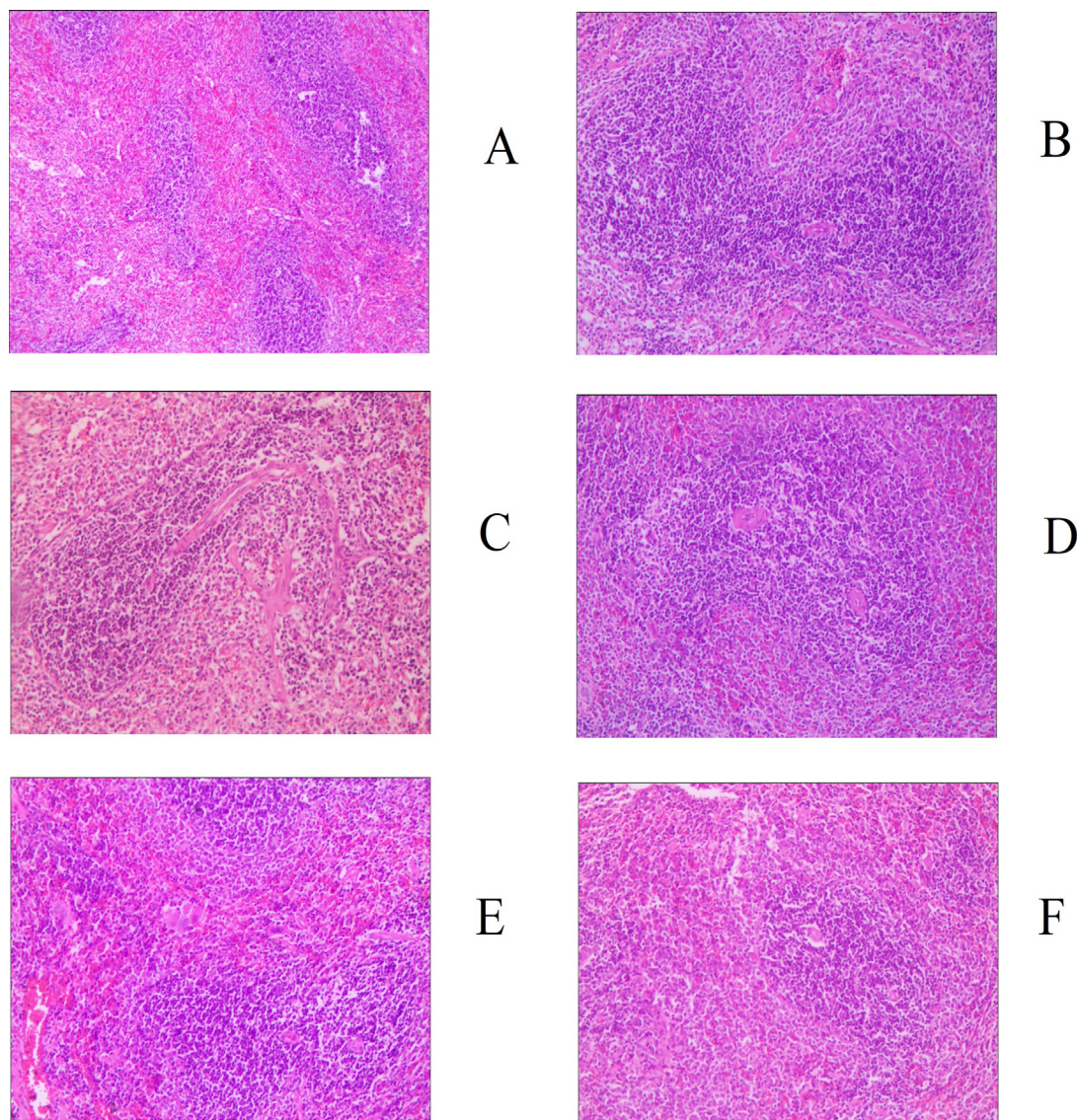


Fig. 4. Histology image of spleen (200x), groups: a. blank, b. serum, c. positive control, d. gyp low dose, e. gyp medium dose, f. gyp high dose.

bolic markers and endow the TCM theoretical basis of GYP with the appropriate biological connotation.

The results of UPLC-TOF-MS and UPLC-MS were selected, and the corresponding variables with $F_c < 0.8$ or $F_c > 1.2$ were used as the main differential metabolites. At the same time, through the primary and secondary mass spectrometry information, combined with the online database HMDB (<https://www.hmdb.ca>), Metlin (<https://metlin.scripps.edu/>), LIPID MAPS and Massbank (<https://www.lipidmaps.org/>) (<https://massbank.eu/MassBank/>) and related literature reports identified, 73 different metabolites were eventually identified in the liver, including 24 upregulated and 49 downregulated metabolites. A total of 147 differential metabolites were found in all matrixes. Through pathway enrichment and topological analysis, the MetaboAnalyst 5.0 database identified the possible metabolic pathways affected by biological perturbation and then analyzed the metabolic pathways of metabolites. The screened differential metabolites were imported into MetaboAnalyst 5.0 database to analyze the related metabolic pathways of the differential metabolites, and the impact of the pathways was obtained by path topology analysis. Combined with

the P of the hypergeometric distribution test, the enrichment results of metabolites were drawn to screen the main metabolic pathways. Pathways with impact values > 0.1 were considered pathways with the largest contribution values. Six common metabolic pathways were screened by serum and organs, including arginine biosynthesis; alanine, aspartic acid and glutamic acid metabolism; D-glutamine and D-glutamic acid metabolism; tryptophan metabolism; ether lipid metabolism; arginine and proline metabolism; and niacin and niacinamide metabolism, as shown in Fig. 9, Fig. S2, Fig. S3.

The relationship between the above metabolites and the PXR/IL-6/SERCA1a pathway can be analyzed by in-depth analysis of metabolic pathways and combined with literature reports to analyze the influence of each metabolite by relevant expression changes. The results showed that a total of 22 endogenous metabolites were closely related to the pathway; the names, m/z , and other information of these metabolites are shown in Table 1. These metabolites were determined by UPLC-MS-MS, and the results showed that the content of the above metabolites in different experimental groups (blank group vs. model/sham operation

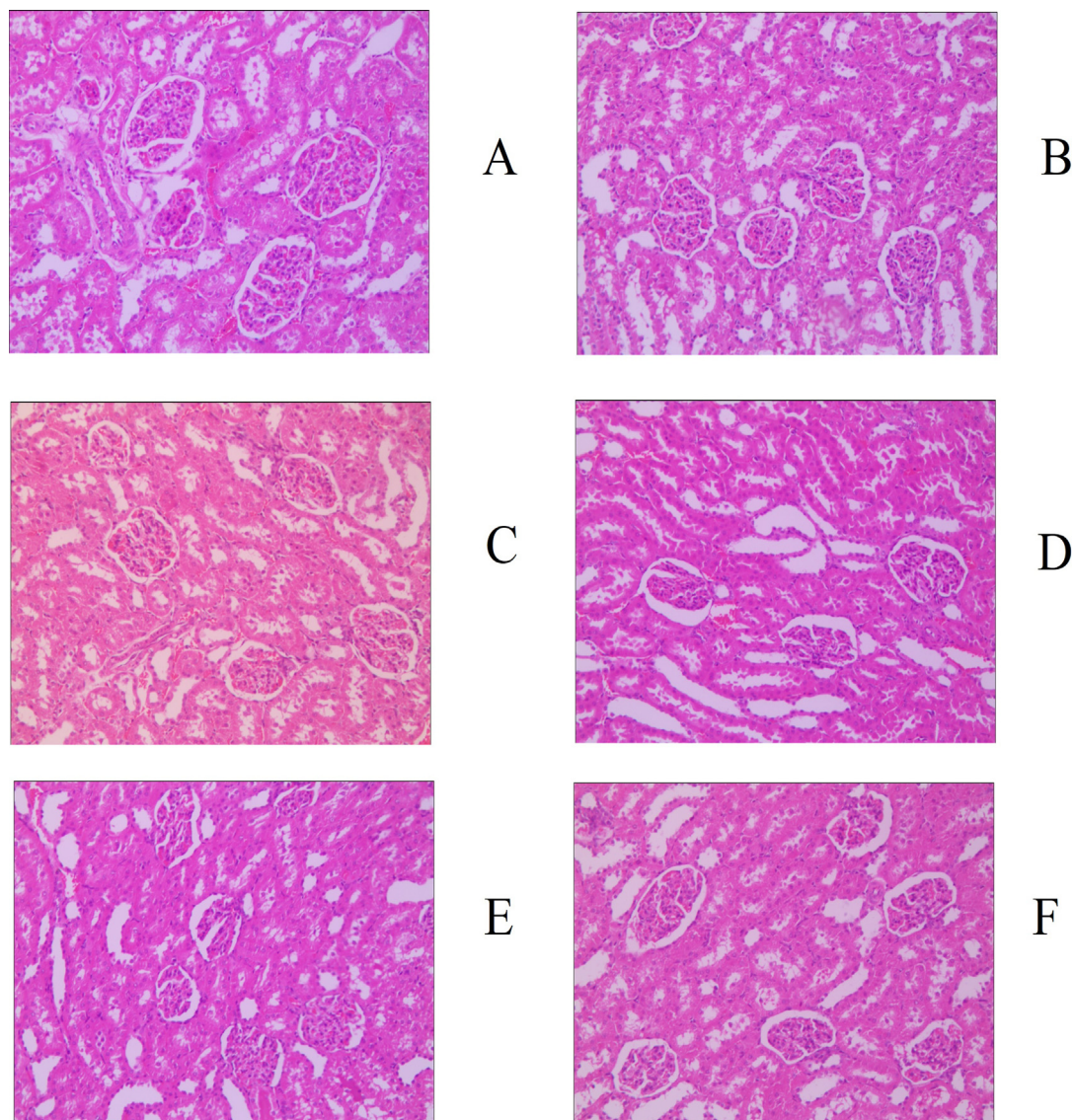


Fig. 5. Histology image of kidney (200x), groups: a. blank, b. serum, c. positive control, d. gyp low dose, e. gyp medium dose, f. gyp high dose.

group, model/sham operation group vs. each treatment group) were significantly different ($p < 0.05$), but the specific differences of each metabolites among the groups were distinct (Fig. 10, Fig. S4, Fig. S5). In the positive control and GYP low-dose groups, there were no significant differences in sphinganine 1-phosphate compared with the sham operation group ($p > 0.05$). However, the above metabolites in the GYP medium- and high-dose groups were significantly different from those in the sham operation group ($p < 0.05$). Additionally, some metabolites in all groups, such as 9-*cis*-retinal, riboflavin, taurocholate, tyrosine, uridine, and xanthine, had no obvious responses in all matrices except the kidney (the value in this organ was low), and some others, such as palmitic acid, had much higher concentrations in skeletal muscle. In general, compared with the blank group, the values of metabolites in each administration group, except the GYP low-dose group, showed a trend of approaching the blank group to different degrees, and more metabolites in the GYP medium- and high-dose groups returned to normal levels than those in the positive drug group.

3.4. Scientific significance of GYP in promoting skeletal muscle strain repair

According to the results obtained in the section “GYP’s influence on skeletal muscle recovery”, GYP’s promoting effect on the recovery of skeletal muscle strain is basically the same as that of the positive control drug. However, the literature reports that researchers have not found strong anti-inflammatory or immune-enhancing effects for GYP (at least not comparable to nonsteroidal anti-inflammatory drugs); that is, the effect of GYP on the repair of injured muscle is mainly attributed to its effects on related pathways such as skeletal muscle regeneration, protein synthesis, substance transport, and energy metabolism. Supplemented by a certain degree of anti-inflammatory activity improves the body’s immune activity (Chen C, et al., 2022; Wang, et al., 2022; Shen, et al., 2019). Through the combined action of the above mechanisms, GYP can accelerate the regeneration of injured skeletal muscle cells, as well as the synthesis of key products such as muscle fibers and muscle lipoproteins, and ultimately promote injury

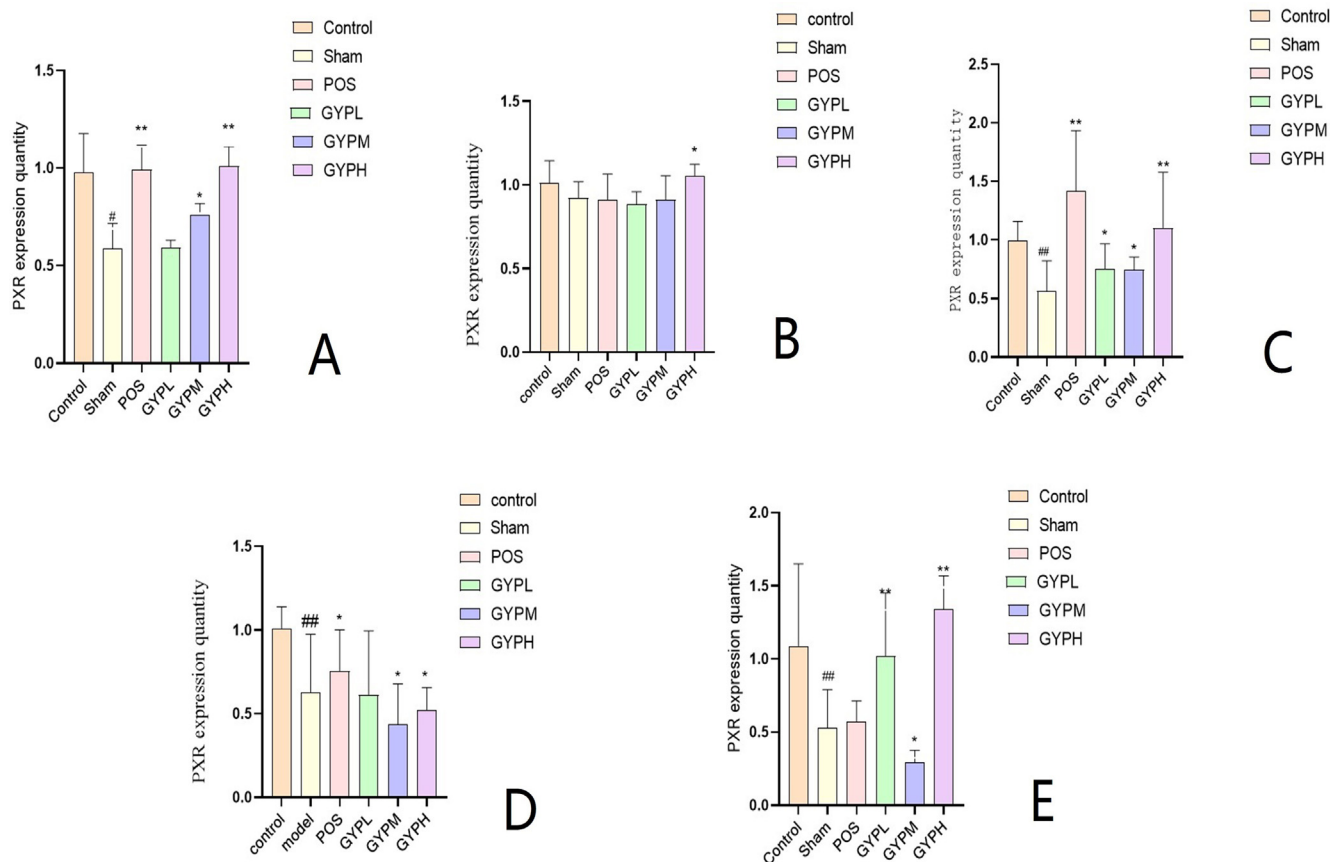


Fig. 6. PXR expression of A. Serum, B. Skeletal muscle, C. Liver, D. Kidney, E. Spleen; Groups: BLK, blank; Sham, sham operation; POS, positive control; GYPL, GYP low dose; GYPM, GYP medium dose; GYPH, GYP high dose.

repair. In contrast, the traditional internal medicine regimen for skeletal muscle injury recovery mainly uses nonsteroidal anti-inflammatory drugs to reduce the inflammatory response and tissue adhesion at the injury site. Although it can also achieve good results (Fig. S2), the side effects of large and long-term use of such drugs are more apparent, and the therapeutic effect of a single mechanism is limited to the recovery ability of the body's overall health level and constitution; it is not as stable, durable, and comprehensive as GYP and other natural products.

3.5. Biological significance of GYP in regulating the PXR/IL-6/SERCA1a pathway

According to the results of the "PXR/IL-6/SERCA1a assay results" section, the expression of PXR in serum and liver tissue of the model group was significantly lower than that of the blank group. Combined with the observation of pathological sections, it can be inferred that the above results may be due to the serious liver injury caused by muscle strain in the model, and PXR is widely distributed in the liver. Functional impairment or impairment of the former can lead to decreased PXR activity (Ge et al., 2022; Liu et al., 2022c). Compared with the model group, PXR expression was increased and restored to different degrees in the GYP treatment groups. At the same time, obvious signs of injury repair could be observed in liver sections, suggesting that GYP plays an overall and comprehensive role in the recovery of the body by regulating physiological function and promoting the repair of metabolic organs such as the liver. The expression of PXR in the skeletal

muscle of each group did not significantly change, which may be related to the lower distribution of the PXR receptor in skeletal muscle and more influencing factors. Therefore, it is difficult to deduce the regulatory mechanism of GYP on PXR simply based on the changes in each group. In addition, PXR, as a nuclear receptor, has a comprehensive regulatory effect on protein, lipid, energy metabolism, and inflammatory factor levels. Combined with our previous results of screening the active components of GYP in promoting skeletal muscle repair, we can conclude that GYP regulates the expression of the PXR receptor through its active components binding to the latter and regulates related physiological functions through changes in expression. Ultimately, the goal is to treat the disease (in this case, to promote repair of strained muscles). In addition, the expression of PXR in various organs was measured in this study (the results are omitted), but the preliminary results showed that there was no obvious pattern of PXR expression in organs such as the kidney and spleen except the liver. The above results are consistent with literature reports that the distribution of PXR is organ specific (Thibaut and Bindels, 2022; Xie et al., 2021), as well as SERCA1a, which is mainly distributed in skeletal muscle and focuses on regulating the latter's function and metabolism. This specificity also influences the IL-6 content. Acting as an indicator of injury and inflammation, this factor varies along with changes in its regulatory receptors. Therefore, the trend of IL-6 variation was relatively correlated with PXR/SERCA1a, with similar organ specificity, which demonstrates its role as an indicator of disease. Moreover, PXR/IL-6/SERCA1a is an important organ of energy and substance metabolism in the body, and PXR/IL-6/

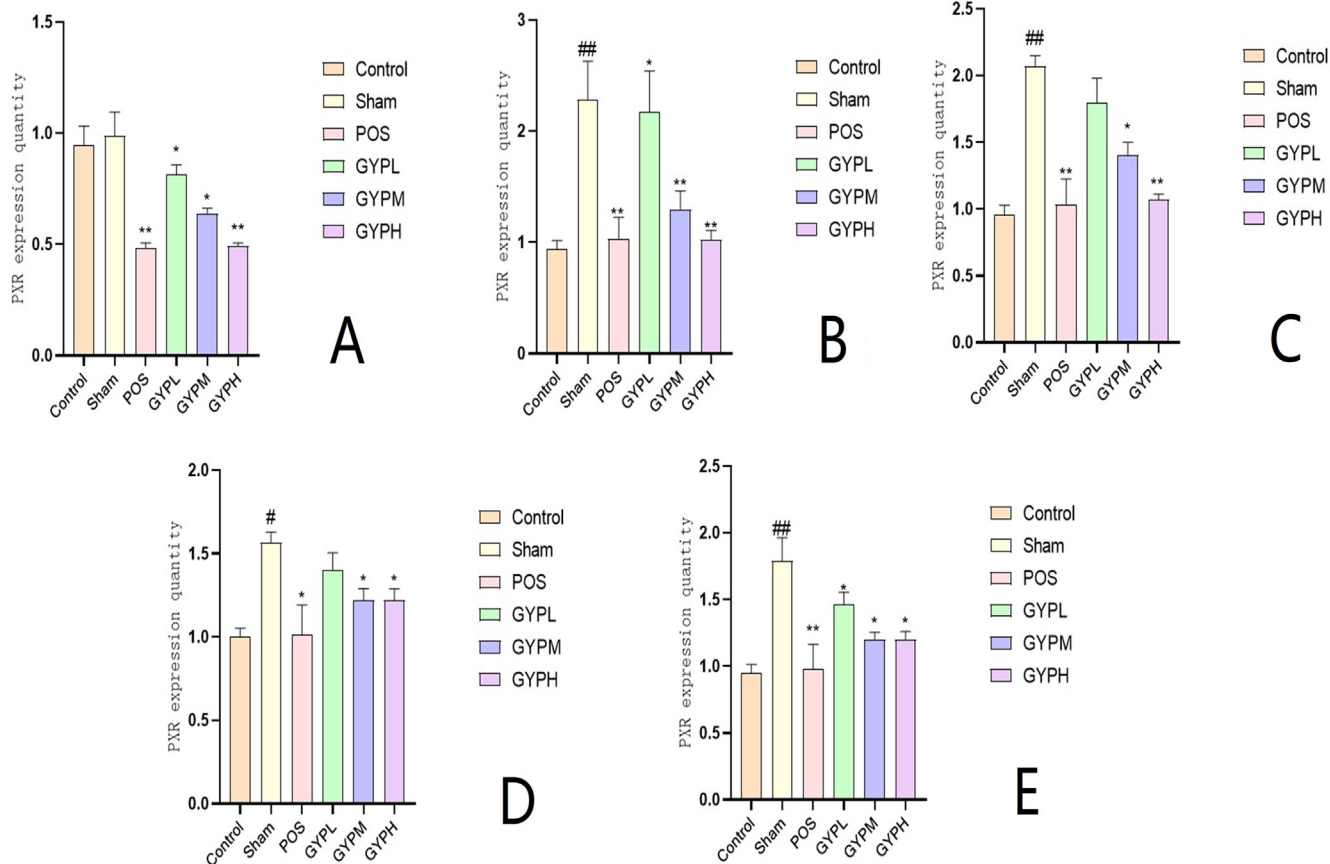


Fig. 7. IL-6 content of A. Serum, B. Skeletal muscle, C. Liver, D. Kidney, E. Spleen; Groups: BLK, blank; Sham, sham operation; POS, positive control; GYPL, GYP low dose; GYPM, GYP medium dose; GYPH, GYP high dose.

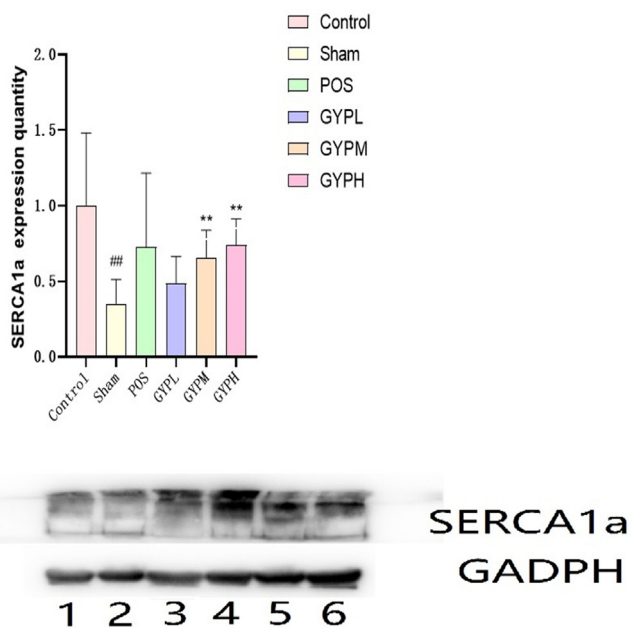


Fig. 8. SERCA1a expression of different groups in skeletal muscle, BLK, blank; Sham, sham operation; POS, positive control; GYPL, GYP low dose; GYPM, GYP medium dose; GYPH, GYP high dose.

SERCA1a expression and its function can better reflect the situation in which this pathway is affected by GYP to regulate the disease course.

3.6. Regulatory mechanisms of GYP on key metabolites in muscle strain repair

PXR has a significant effect on the level, transport and distribution of inflammatory factors in vivo. It has been found that this receptor can interact with NF-κB, and change the concentration of downstream physiological factors such as IL-6, IL-1β, IL-10 and TNF-α by affecting the activity of the latter, so as to reduce inflammation and pain response at the injured site (Bautista-Olivier, et al., 2022). At the same time, IL-6 can also affect the activity of SERCA1a, which is mainly distributed in skeletal muscle, and its functions are mainly involved in energy metabolism, motor function and apoptosis inhibition, etc. PXR has direct and indirect effects on this site, and the former is mediated by inflammatory factors such as IL-6. The latter indirectly regulates the concentration and activity of SERCA1a ligand by changing the activities of heat production, energy metabolism and material transport organs such as liver, kidney, spleen and small intestine (Nelson, et al., 2016; Pant, et al., 2016).

Through the analysis of metabolomics results (Figs. 1, 9, Figs. S2–S5), database signal pathway analysis results and

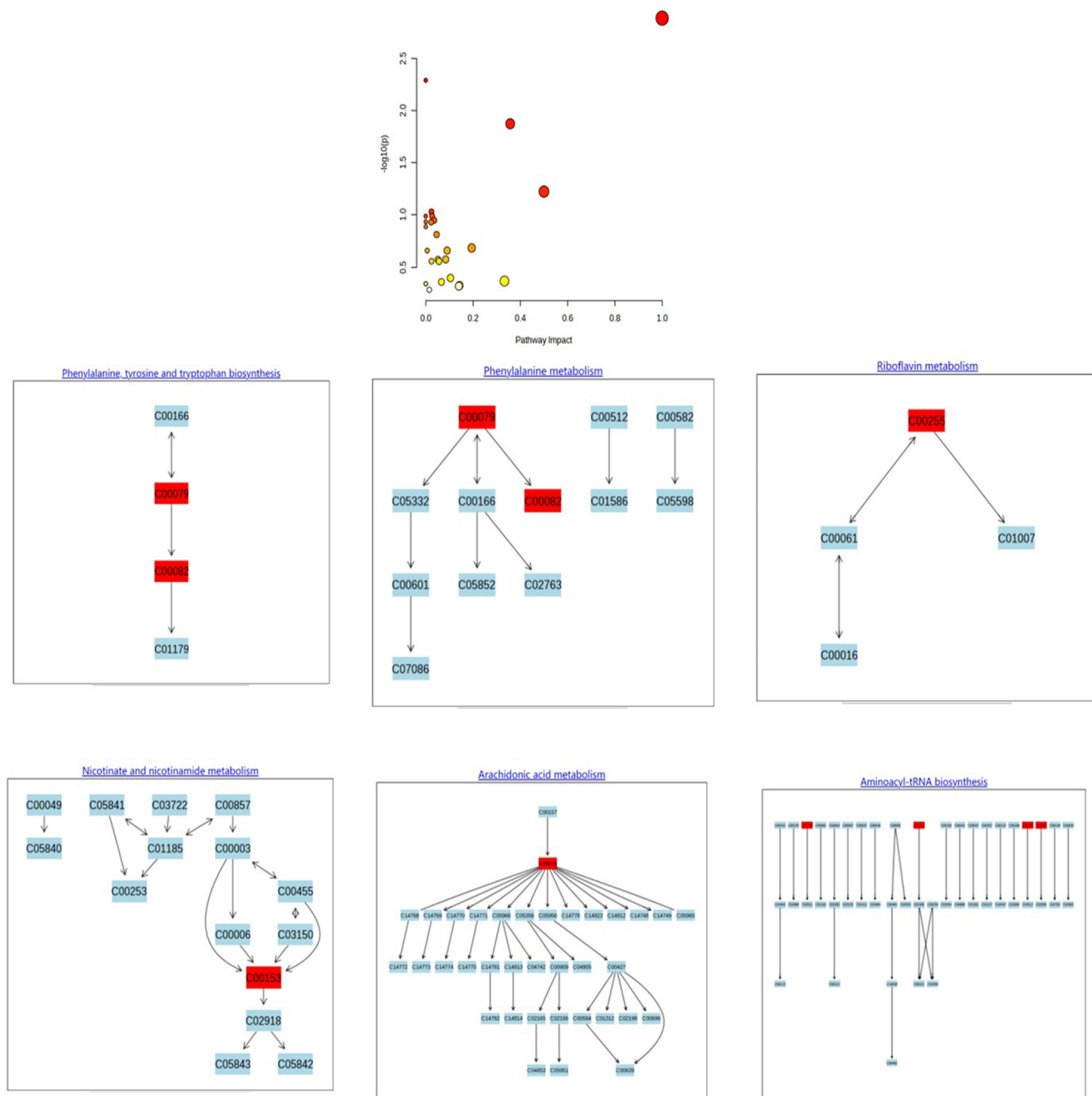


Fig. 9. Overview of the metabolomic pathway.

literature reports, the changes in related metabolites under GYP intervention were mainly involved in the synthesis and transformation of multiple amino acids in vivo (Gandhi et al., 2020; Zhang et al., 2013). Among them, the D-glutamine pathway regulates the activities of various proteins and enzymes in the body and can be involved in gluconeogenesis. At the same time, the metabolic pathway of SERCA1a can regulate the production of glutamate, which is an important energy provider for cell growth and differentiation, regulating calcium ion concentration inside and outside the sarcoplasmic reticulum, stimulating Ca²⁺ influx and ATP metabolism, accelerating muscle tissue growth, and promoting muscle recovery. According to the above content, the D-glutamine metabolism pathway is closely related to SERCA1a activity (Junaidi, et al., 2022; Sawant, et al., 2020; Qaisar et al.,

2019). In addition to energy supply, alanine, aspartate, glutamate, and other amino acid metabolic pathways, in which glutamate can also generate glutathione, remove oxygen free radicals infiltrated by cells, eliminate inflammation, protect cells, and promote muscle repair (Devignes, et al., 2022; Suzuki and Iwata, 2021). Studies have shown that activated PXR can affect the levels of inflammatory factors by regulating IL-6. In this study, it can be reflected in the effect on the tryptophan metabolism pathway. The bio-transformation of this metabolite can regulate liver lipid metabolism, inhibit the activity of fat synthetase, reduce intrahepatic triglyceride and lipid synthesis, increase liver fatty acid oxidation and cellular uptake of glucose, avoid fat accumulation in hepatocytes, reduce the level of inflammatory factors and inhibit the inflammatory response. At the same time, tryptophan is also

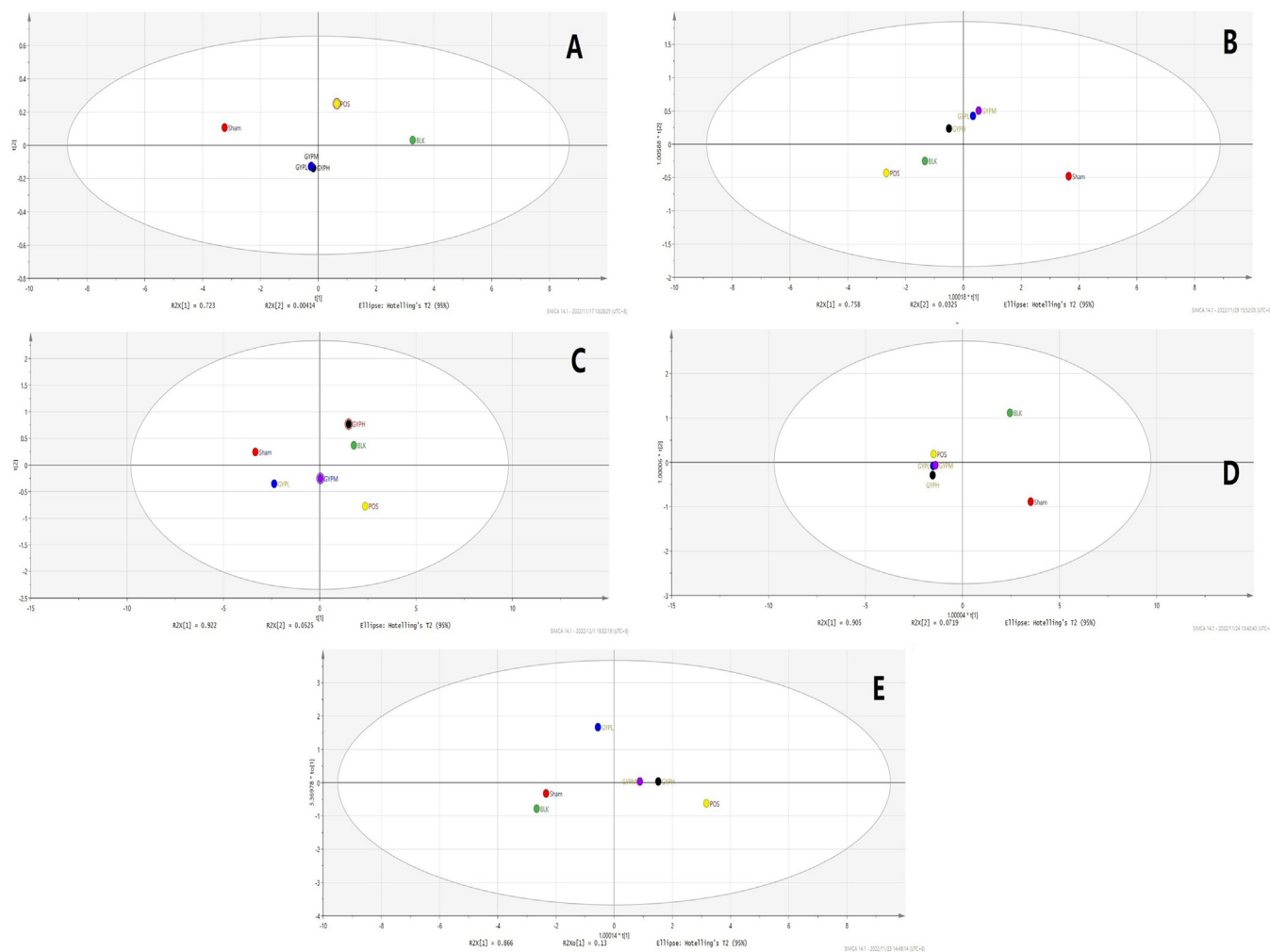


Fig. 10. OPLS-DA analysis of each group (including both negative and positive ions), A. Serum, B. Skeletal muscle, C. Liver, D. Kidney, E. Spleen; Groups: BLK, blank; Sham, sham operation; POS, positive control; GYPL, GYP low dose; GYPM, GYP medium dose; GYPH, GYP high dose.

the raw material for protein synthesis. Tryptophan regulates lipid metabolism in the body and can stimulate the release of insulin and increase the synthesis of protein in muscle and liver, which can promote the synthesis of protein in muscle and restore damaged muscle (Zhang, et al., 2020; Wang and Li, 2019; Hassani-Nezhad-Gashti, et al., 2018; Wu, et al., 2018; Ihunnah, et al., 2011). In addition, the PXR/IL-6 pathway can also reduce the expression of genes related to fat and glycogen synthesis by regulating arginine metabolism, change the expression of genes related to the oxidation and decomposition of fatty acids to water and CO₂, accelerate fat metabolism, promote lipolysis (Hong, et al., 2022; Javrushtyan, et al., 2022), and provide energy for muscle injury repair. In conclusion, the effects of GYP on PXR/IL-6/SERCA1a exerted both enhanced and accelerated metabolic effects, which could increase lipid metabolism and energy supply, accelerate muscle cell regeneration and protein synthesis during muscle injury/strain repair, and provide more energy for these processes.

The biological relationship between GYP regulating the changes in PXR/IL-6/SERCA1a and related metabolites and the effect of Tonic deficiency in both the spleen and kidney.

Based on the results of animal experiments, molecular biology, and metabolomic studies; GYP can regulate the metabolism of cells and tissues related to skeletal muscle cells and muscle fibrin and provide sufficient energy for this process. According to the classical theory of traditional Chinese medicine, the kidney is dominated by

bone, and the spleen is dominated by muscle (Jiang and Zou, 2013). The pathological section observation showed that the above two organs were significantly recovered under the action of GYP compared with the model group. The observation results at the microscopic level were also consistent with the above macro results: the expression of IL-6 in the spleen in the medium-dose GYP and high-dose GYP groups was significantly lower than that in the model group, and the level of related endogenous metabolites basically recovered to normal. In addition, the morphology and metabolic function of the liver showed a recovery trend after GYP intervention, both at the macro and micro levels. The latter regulates the energy supply and substance metabolism of the former, especially the proteins and amino acids related to damage repair, which corresponds to the effects of toning deficiency, invigorating the spleen (called warming middle Jiao TCM theory), and toning the kidney in traditional Chinese medicine theory (Yang and Pei, 2023; Zhang, et al., 2022; Huang, et al., 2020). At the skeletal muscle level, muscle tissue recovery, SERCA1a expression and related metabolite level increases under GYP intervention can be associated with the muscle strengthening effect of GYP. At the same time, since the metabolic markers determined in this study are closely related to the PXR/IL-6/SERCA1a signaling pathway, the precise determination method of metabolites established in this paper provides a quantifiable standard for evaluating the abovementioned efficacy of GYP in traditional Chinese medicine.

4. Conclusion

In this paper, the mechanism of PXR/IL-6/SERCA1a-mediated muscle injury repair under GYP intervention was studied deeply and comprehensively, the efficacy mechanism of GYP in toning spleen and liver deficiency was clarified, and a number of endogenous metabolic markers related to the disease course and drug treatment were found. At the same time, by integrating the above experimental and analytical data, we offer a biological basis for the TCM efficacy of GYP. In summary, these results provide a basis for scientific and systematic interpretation of the therapeutic basis of GYP and contribute to the subsequent development of this medicine and deeper mechanistic research.

Declaration of competing interest

The authors declare that they have no known competing financial interests or personal relationships that could have appeared to influence the work reported in this paper.

Acknowledgements

The authors thank National Natural Science Foundation of China (number 81903761) and the Scientific Research Project of Traditional Chinese Medicine Bureau of Guangdong Province (number 20231108) for their financial and policy support.

Appendix A. Supplementary material

Supplementary data to this article can be found online at <https://doi.org/10.1016/j.arabjc.2023.105293>.

References

Alhasani, R., Zhou, X., Biswas, L., 2020. Gypenosides attenuate retinal degeneration in a zebrafish retinitis pigmentosa model. *Experimental Eye Res.* 201, 108291.

Bautista-Olivier, C., Elizondo, G., 2022. PXR as the tipping point between innate immune response, microbial infections, and drug metabolism. *Biochem. Pharmacol.* 202, (1) 115147.

Biagioli, M., Fiorucci, S., 2021. Bile acid activated receptors: Integrating immune and metabolic regulation in non-alcoholic fatty liver disease. *Liver Res.* 5 (3), 119–141.

Bitman, M., Dvorak, Z., Vrzal, R., Stejskalová, L., Pávek, P., 2011. The cross-talk of extracellular signal-regulated protein kinase (ERK) and pregnane X receptor (PXR) and its effect on expression of CYP3A4 and MDR1 genes in primary human hepatocytes and hepatoma cell lines. *Toxicology Let.* 205, 2366.

Camejo, F.D.A., Doetzer, A., Haxhia, A., Herm, L., Almeida, L.E., Trevilatto, P.C., 2020. Correlation between FasL and IL-6 Expression in Human TMJ Disks with and without Osteoarthritis. *J. Oral Maxillofac. Surg.* 78 (10), e100.

Cao, H., Xiao, G., Li, D., Chen, X., Chen, W., Chen, Z., 2022. Gynostemma pentaphyllum promotes skeletal muscle recovery via its inhibition of PXR-IL-6 expression. *Phytomed. Plus* 2, (1) 100305.

Chen, Q., Fan, Z., Lyu, A., Wu, J., Guo, A., Yang, Y., Chen, J., Xiao, Q., 2020. Effect of sarcosine-mediated cell trans differentiation in sarcopenia associated skeletal muscle fibrosis. *Exper. Cell Res.* 389, (1) 111890.

Chen, C., Fu, D., Wu, Y., Huang, C., Huang, P., 2022a. Gypenoside, the main active compound of *Gynostemma pentaphyllum*, mitigates the Diabetic Nephropathy through down-regulating mTOR. *Clin. Complement. Med. & Pharmacol.* 2, (3) 100060.

Chen, Z., Li, D., Li, X., Xiao, G., Bi, X., Chen, W., Shi, Z., Zeng, X., Sun, D., Cao, L., 2021. The anti-hyperlipidemia effect of Yinlan capsule via regulation of PXR activity. *Phytomed. Plus* 1, (1) 100086.

Chen, S., Liu, X., Zhao, H., Cheng, N., Sun, J., Cao, W., 2022b. Beneficial effects of *Gynostemma pentaphyllum* honey paste on obesity via counteracting oxidative stress and inflammation: an exploration of functional food developed from two independent foods rich in saponins and phenolics. *Food Res. Int.* 157, 111483.

Devignes, C., Carmeliet, G., Stegen, S., 2022. Amino acid metabolism in skeletal cells. *Bone Rep.* 17, 101620.

Gandhi, G., de Sousa Leão, G., da Silva Calisto, V., Vasconcelos, A., Almeida, M., de Souza Siqueira Quintans, J., Barreto, E., Narain, N., Júnior, L.S., Gurgel, R., 2020. Modulation of interleukin expression by medicinal plants and their secondary metabolites: a systematic review on anti-asthmatic and immunopharmacological mechanisms. *Phytomed.* 70.

Ge, J., Huang, Y., Lv, M., Zhang, C., Talukder, M., Li, J., Li, J., 2022. Cadmium induced Fak-mediated anoikis activation in kidney via nuclear receptors (AHR/CAR/PXR)-mediated xenobiotic detoxification pathway. *J. Inorganic Biochem.* 227, 111682.

Hakkola, J., Rysä, J., Hukkanen, J., 2016. Regulation of hepatic energy metabolism by the nuclear receptor PXR. *BBA - Gene Regulatory Mechanisms* 1859 (9), 1072–1082.

Hassani-Nezhad-Gashti, F., Rysä, J., Kummua, O., et al., 2018. Activation of nuclear receptor PXR impairs glucose tolerance and dysregulates GLUT2 expression and subcellular localization in liver. *Biochem. Pharmacol.* 148 (1), 253–264.

Hong, W., Peng, X., Zhou, X., Li, P., Ye, Z., Liang, W., 2022. FXR/ASS1 axis attenuates the TAA-induced liver injury through arginine metabolism. *Biochem. Biophys. Res. Commun.* 611, 31–37.

Huang, L., Ye, M., Wu, J., Liu, W., Chen, H., Rui, W., 2020. A metabonomics and lipidomics based network pharmacology study of qi-tonifying effects of honey-processed *Astragalus* on spleen qi deficiency rats. *J. Chromatogr. B* 1146, 122102.

Ihunnah, C., Jiang, M., Xie, W., 2011. Nuclear receptor PXR, transcriptional circuits and metabolic relevance. *BBA* 1812, 956–963.

Ilaivi, A., ten Have, G., Bain, J., Muehlbauer, M., O'Neal, S., Berthiaume, J., Parry, T., Deutz, N., Willis, M., 2019. Identification of metabolic changes in ileum, jejunum, skeletal muscle, liver, and lung in a continuous I.V. *Pseudomonas aeruginosa* model of sepsis using nontargeted metabolomics analysis. *Amer. J. Pathol.* 189 (9), 1797–1813.

Javrushyan, H., Nadiryan, E., Grigoryan, A., Avtandilyan, N., Maloyan, A., 2022. Antihyperglycemic activity of L-norvaline and L-arginine in high-fat diet and streptozotocin-treated male rats. *Exp. Mol. Pathol.* 126, 104763.

Jiang, P., Wang, L., Zhang, M., Zhang, M., Wang, C., Zhao, R., Guan, D., 2020. Cannabinoid type 2 receptor manipulates skeletal muscle regeneration partly by regulating macrophage M1/M2 polarization in IR injury in mice. *Life Sci.* 256, 117989.

Jiang, Y., Zou, J., 2013. Analysis of the TCM theory of traditional Chinese health exercise. *J. Sport Health Sci.* 2 (4), 204–208.

Junaidi, N., Clément-Vidal, A., Flori, A., Syafaah, A., Oktavia, F., Ismawanto, S., Aji, M., Subandiyah, S., Montoro, P., 2022. Analysis of reduced and oxidized antioxidants in *Hevea brasiliensis* latex reveals new insights into the regulation of antioxidants in response to harvesting stress and tapping panel dryness. *Heliyon* 8 (7), e09840.

Kaur, S., Bansal, Y., Kumar, R., et al., 2020. A panoramic review of IL-6: Structure, pathophysiological roles and inhibitors. *Bioorganic Medicinal Chem.* 28, (5) 115327.

Kumar, M., Muthu, P., 2015. Sarcosine is a novel regulator of muscle metabolism and obesity. *Pharmacol. Res.* 102, 270–275.

Liu, P., Jiang, L., Kong, W., Xie, Q., Li, P., Liu, X., Zhang, J., Liu, M., Wang, Z., Zhu, L., Yang, H., Zhou, Y., Zou, J., Liu, X., Liu, L., 2021c. PXR activation impairs hepatic glucose metabolism partly via inhibiting the HNF4 α -GLUT2 pathway. *Acta Pharm. Sin. B* 12 (5), 2391–2405.

Liu, H., Li, X., Duan, Y., Xie, J., Piao, X., 2021b. Mechanism of gypenosides of *Gynostemma pentaphyllum* inducing apoptosis of renal cell carcinoma by PI3K/AKT/mTOR pathway. *J. Ethnopharmacol.* 271, 113907.

Liu, Y., Ma, J., Cui, D., Fei, X., Lv, Y., Lin, J., 2020. LncRNA MEG3-210 regulates endometrial stromal cells migration, invasion and apoptosis through p38 MAPK and PKA/SERCA2 signalling via interaction with Galectin-1 in endometriosis. *Mole. & Cell. Endocrinol.* 513, 110870.

Liu, F., Yao, Y., Lu, Z., Zhang, Q., Liu, C., Zhu, C., Lin, C., 2021a. 5-Hydroxy-4-methoxycanthin-6-one alleviates dextran sodium sulfate-induced colitis in rats via regulation of metabolic profiling and suppression of NF- κ B/p65 signaling pathway. *Phytomed.* 82, 153438.

Nelson, B., Makarewicz, C., Anderson, D., Winders, B., Troupes, C., Wu, F., Reese, A., McAnally, J., Chen, X., Kavalali, E., Cannon, S., Houser, S., Bassel-Duby, R., Olson, E., 2016. A peptide encoded by a transcript annotated as long noncoding RNA enhances SERCA activity in muscle. *Science* 351 (6270), 271–275.

Oliva, A., García-Carrillo, S., Ortiz, A., Aranda, F., Teruel, J., 2021. Interaction of a dirhamnolipid biosurfactant with sarcoplasmic reticulum calcium ATPase (SERCA1a). *Arch. Biochem. Biophys.* 699, 108764.

Panci, G., Chazaud, B., 2021. Inflammation during post-injury skeletal muscle regeneration. *Semin. Cell Dev. Biol.* 119, 32–38.

Pant, M., Naresh, C., Bal, P., Periasamy, M., 2016. Sarcosine: a key thermogenic and metabolic regulator in skeletal muscle. *Trends Endocrinol. Metab.* 27 (12), 882–892.

Qaisar, R., Bhaskaran, S., Ranjit, R., Sataranatarajan, K., Premkumar, P., Huseman, K., Van Remmen, H., 2019. Restoration of SERCA ATPase prevents oxidative stress-related muscle atrophy and weakness. *Redox Biol.* 20, 68–74.

Sawant, O., Meng, C., Wu, G., Washburn, S., 2020. Prenatal alcohol exposure and maternal glutamine supplementation alter the mTOR signaling pathway in ovine fetal cerebellum and skeletal muscle. *Alcohol* 89, 93–102.

Shen, C., Shi, M., Yang, H., et al., 2019. Inhibitory effects of multi-components from *Gynostemma pentaphyllum* (Thunb.) Makino on macrophage foam cell formation exhibit multi-target characteristics. *J. Func. Foods.* 60, 103451.

Sikorska, M., Dutkiewicz, M., Zegrocka-Stendel, O., Kowalewska, M., Grabowska, I., Koziak, K., 2021. Beneficial effects of β -escin on muscle regeneration in rat model of skeletal muscle injury. *Phytomed.* 93, 153791.

Suzuki, A., Iwata, J., 2021. Amino acid metabolism and autophagy in skeletal development and homeostasis. *Bone* 146, 115881.

Tanihata, J., Nagata, T., Ito, N., Saito, T., Nakamura, A., Minamisawa, S., Aoki, Y., Ruegg, U.T., Takeda, S.I., 2018. Truncated dystrophin ameliorates the dystrophic

- phenotype of mdx mice by reducing sarcolipin-mediated SERCA inhibition. *Biochem. Biophys. Res. Commun.* 505 (1), 51–59.
- Thibaut, M., Bindels, L., 2022. Crosstalk between bile acid-activated receptors and microbiome in entero-hepatic inflammation. *Trends in Mole. Med.* 28 (3), 223–236.
- Ticho, A., Malhotra, P., Dudeja, P., Gill, R., Alrefai, W., 2019. Bile acid receptors and gastrointestinal functions. *Liver Res.* 3, 31–39.
- Wang, X., Li, W., 2019. Changes of serum inflammatory factors and miR-145 expression in patients with osteoarthritis before and after treatment and their clinical value. *World J Clin Case.* 7 (19), 2963–2975.
- Wang, J., Meng, X., Wang, W., Sang, C., Ha, T., Yang, J., 2022. Dammarane triterpenoids with rare skeletons from *Gynostemma pentaphyllum* and their cytotoxic activities. *Fitoterapia* 162, 105280.
- Weng, X., Lou, Y., Wang, Y., 2021. New dammarane-type glycosides from *Gynostemma pentaphyllum* and their lipid-lowering activity. *Bioorg. Chem.* 111, 104843.
- Won, K., Park, J., Jeong, H., 2019. Repression of hepatocyte nuclear factor 4 alpha by AP-1 underlies dyslipidemia associated with retinoic acid. *J. Lip. Res.* 60, 794–804.
- Wu, T., Chan, S., Chang, C., Yu, P., Chuang, C., Yeh, S., 2018. Quercetin and chrysin inhibit nickel-induced invasion and migration by downregulation of TLR4/NF- κ B signaling in A549 cells. *Chemico-Biol. Interac.* 292, 101–109.
- Xie, A., Mai, C., Zhu, Y., Liu, X., Xie, Y., 2021. Bile acids as regulatory molecules and potential targets in metabolic diseases. *Life Sci.* 287, 120152.
- Yang, X., Pei, X., 2023. Comparative efficacy of tonifying kidney on treatment of mammary gland hyperplasia: systematic review with network meta-analysis. *Phytomedicine Plus.* 3, (1) 100395.
- Yang, Y., Yang, J., Jiang, Q., 2013. Hypolipidemic effect of gypenosides in experimentally induced hypercholesterolemic rats. *Lipids in Health & Dis.* 12, 154–160.
- Yue, Z., Nie, A., Chen, S., Wang, M.e., Yin, R., Tang, B., Wu, Y., Yang, F., Du, B., Shi, H., Yang, X., Hao, G., Guo, X., Han, Q., Zheng, Y., Zhao, W., 2021. Downregulation of renal MRPs transporters in acute lymphoblastic leukemia mediated by the IL-6/STAT3/PXR signaling pathway. *J. Inflamm. Res.* 14, 2239–2252.
- Zhang, X., Bi, X., Xiao, W., Cao, J., Xia, X., Diao, Y., Zhao, Y., 2013. Protein tyrosine phosphatase 1B inhibitory effect by dammarane-type triterpenes from hydrolyzate of total *Gynostemma pentaphyllum* saponins. *Bioorg. Med. Chem. Lett.* 23 (1), 297–300.
- Zhang, G., Liu, M., Song, M., Wang, J., Cai, J., Lin, C., Li, Y., Jin, X., Shen, C., Chen, Z., Cai, D., Gao, Y., Zhu, C., Lin, C., Liu, C., 2020. Patchouli alcohol activates PXR and suppresses the NF- κ B-mediated intestinal inflammatory. *J. Ethnopharmacol.* 248, 112302.
- Zhang, Q., Wang, X., Yan, G., Lei, J., Zhou, Y., Wu, L., Wang, T., Zhang, X., Ye, D., Li, Y., 2018. Anti- versus pro-inflammatory metabololipidome upon cupping treatment. *Cell. Physiol. Biochem.* 45, 1377–1389.
- Zhang, J., Wang, X., Wang, F., Tang, X., 2022. Xiangsha Liujuanzi Decoction improves gastrointestinal motility in functional dyspepsia with spleen deficiency syndrome by restoring mitochondrial quality control homeostasis. *Phytomedicine* 105, 154374.
- Zhou, Z., Qi, J., Zhao, J., Seo, J., Shin, D., Cha, J., Lim, C., Kim, J., Kim, B., 2021. *Orostachys japonicus* ameliorates acetaminophen-induced acute liver injury in mice. *J. Ethnopharmacol.* 265, 113392.